Composites: Part B 59 (2014) 269–278

Contents lists available at ScienceDirect

Composites: Part B

journal homepage: www.elsevier.com/locate/compositesb

Free vibration of FGM layered beams by various theories and finite elements

Daoud S. Mashat [a], E. Carrera [a,b], Ashraf M. Zenkour [a,c], Sadah A. Al Khateeb [a], M. Filippi [b,*]

[a] Department of Mathematics, Faculty of Science, King Abdulaziz University, P.O. Box 80203, Jeddah 21589, Saudi Arabia
[b] Department of Mechanical and Aerospace Engineering, Politecnico di Torino, Italy
[c] Department of Mathematics, Faculty of Science, Kafrelsheikh University, Kafr El-Sheikh 33516, Egypt

ARTICLE INFO

Article history:
Received 24 October 2013
Accepted 7 December 2013
Available online 20 December 2013

Keywords:
A. Layered structures
B. Mechanical properties
B. Vibration
C. Finite element analysis (FEA)

ABSTRACT

The Carrera Unified Formulation (CUF) is used to perform free-vibrational analyses of functionally graded (FG) structures. CUF is a hierarchical formulation for obtaining refined structural theories that account for variable kinematic description. These theories can be obtained by expanding the unknown displacement variables over the beam section axes by adopting any kind of function. The number of the terms in the expansions is a free parameter of the analysis. For Taylor-like expansions, the linear case can result in classical beam theories. For the first time in the 1D CUF framework, the Finite Element method is used to solve the governing equations of functionally graded beams which are derived in a weak form by means of the Principle of Virtual Displacements. These equations are written in terms of fundamental nuclei. Their forms do not depend on the expansions used. Several structures are considered, including a sandwich beam with FG core, laminated beams, thin- and thick-walled boxes as well as sandwich cylinders. The results are shown in terms of natural frequencies and compared with those available in existing literature.

1. Introduction

In recent years, functionally graded materials (FGMs) have gained great attention in many engineering fields, especially when the structures are subjected to high temperatures. The smooth variation of the mechanical properties along preferential directions is achieved by changing the volume fractions of two or more constituent materials, which are generally ceramic and metal(s). By doing this, the well-known problems of the classical composite materials, such as the discontinuities of the stress distributions at the interfaces and the low resistance to temperature shocks, can be avoided. In addition, the behaviour of these materials strongly depends on the gradation law which is used and for this reason, many theoretical models are conceived in order to describe the FG structures properly. Among the several beam theories available in the literature, in [1] Aydogdu and Vedat presented a comparison between different displacement fields for the free vibration zanalysis of simply supported structures. For the same boundary condition, Thai and Vo also carried out a static analysis [2]. Other configurations were considered in [3], where Şimşek used the Lagrange multipliers for analyzing beams with different boundary conditions. Many researchers have also extended the classical beam theories to the study of FGM. For instance, Li proposed a unified approach to study the nonhomogeneous beams and with this method both Euler and Rayleigh models were obtained using the Timoshenko theory. Some interesting comparisons between these theories and a number of results were presented in terms of deflections, stress distributions and natural frequencies [4]. A further example is [5], in which Sina and Navazi derived the equations of motion of FG beams by adopting a modified first-order shear deformation theory and solved them with an analytical method. The authors showed how the boundary conditions, the volume fractions and the shear deformation affect the natural frequencies as well as the modal shapes. Recently, Pradhan and Chakraverty [6] obtained the equations of motion by means of the Rayleigh–Ritz method in which the vibration amplitudes are expanded in terms of algebraic polynomial functions. The authors considered many conditions and validated their solution with the available results from the existing literature. Even complex structures were analyzed by using a first-order shear deformation theory. For example in [7], Ziane et al. developed a theory which included the shear deformation as well as the primary and the secondary torsional warping for studying thin and thick-walled FGM box beams. The results were obtained by the Dynamic Stiffness Method and validated with Finite Element solutions. For multi-layer, a number of *ad hoc* models have been proposed. For instance, in [8], Kapuria et al. presented a third order zig-zag displacement theory in

* Corresponding author. Tel.: +39 011 090 6870.
E-mail address: matteo.filippi@polito.it (M. Filippi).

1359-8368/$ - see front matter © 2013 Elsevier Ltd. All rights reserved.
http://dx.doi.org/10.1016/j.compositesb.2013.12.008

conjunction with the modified rule of mixture for the static and dynamic analysis. The results were validated through interesting experiments. Furthermore, Rahmani et al. studied the behaviour of sandwich beams with syntactic foam and considered the core as a functionally graded material [9]. Their model is based on a high-order sandwich panel theory which takes into account the flexibility of the core. The results are only available for the simply-supported structures. Further dynamic analysis of sandwich beams were performed in [10,11], in which the Galerkin method and the radial point interpolation procedure were adopted, respectively. The results were compared with those obtained by alternative methods, including the Finite Element method.

In addition to the above papers, many two-dimensional theories have appeared in recent literature for the study of plates and shells containing FGMs. For example, Reddy and co-workers provided the first results on the vibration of FG plates and cylindrical shells in [12–14]. Static and dynamic analyses were performed on thick plates by using a higher-order shear and normal deformable plate theory in [15]. This work was the reference for the results shown in [16], in which the authors used the radial basis functions with the first and third-order shear deformation theories. Matsunaga [17] also investigated the stability and the dynamic features of the FG simply-supported plates by using the method of power expansion of displacement components. These higher-order models accurately predict the natural frequencies, the critical load and the stress distributions. Further examples were presented in [18,19], in which the generalized differential quadrature method was adopted for analyzing the completely doubly curved and degenerate shells. In [19], the authors applied two different optimization approaches to define the mixture for optimizing the first natural frequency and the static deflection of the considered structures.

The main scope of this work is to evaluate several refined beam finite elements. These higher-order theories are obtained by means of the Carrera Unified Formulation (CUF). CUF is a well-known procedure, which was initially conceived for the development of refined plate and shell theories [20] and later extended to beam formulation [21]. CUF has been extensively used for dealing with a wide range of structural problems including, for instance, the static and dynamic analysis of composite structures [22,23], the free vibration analysis of rotating beams [24] and the study of the mechanical behaviour of structures with unconventional cross-sections [25–27]. In particular, for the dynamic behaviour of FG structures, the unified formulation was used by Cinefra and Soave [28] and Dozio [29], which proposed a closed-form solution for the simply-supported multilayered plates and two advanced Ritz-based models, respectively. In addition to these two works, adopting a closed form solution, Giunta and co-workers assessed the higher-order displacement models for the free vibration problem of simply-supported FG beams [30].

In the present work, by using the Finite Element method several FG structures under various boundary conditions are considered. The displacement components are defined by using a variety of functions such as polynomial, trigonometric, hyperbolic and exponential. The study focuses on laminated and sandwich structures as well as thin-walled boxes, in which the mechanical properties vary according to the typical power gradation law. The results are reported in terms of natural frequencies and they are compared with those existing in the literature.

2. The Carrera unified formulation

The CUF states that the displacement field, $\boldsymbol{u}(x,y,z,t)$, is an expansion of generic functions, $F_\tau(x,z)$ for the vector displacement, $\boldsymbol{u}_\tau(y)$:

$$\boldsymbol{u}(x,y,z,t) = F_\tau(x,z)\boldsymbol{u}_\tau(y,t) \qquad \tau = 1,2,\ldots,T \tag{1}$$

where T is the number of terms of the expansion and, according to the generalized Einstein's notation, τ indicates summation. The main advantage of the present approach is that it considers both type and number of functions $F_\tau(x,z)$ as input parameters. Therefore, the number of higher-order theories which can be generated is theoretically infinite. In previous papers, encouraging results were obtained by using several advanced theories based on trigonometric, exponential, polynomials and miscellaneous expansions for the study of composite structures. For a thorough and clear description of the new displacement theories, the authors suggest [22,23]. An example of a displacement model which can be used is the following:

$$\begin{aligned}
u_x &= u_{x_1} + x\,u_{x_2} + z\,u_{x_3} + x^2\,u_{x_4} + xz\,u_{x_5} + z^2 + e^{\left(1\frac{x}{a}\right)}u_{x_6} + e^{\left(1\frac{z}{b}\right)}u_{x_7} + \sin\left(3\frac{\pi x}{a}\right)u_{x_8}\\
u_y &= u_{y_1} + x\,u_{y_2} + z\,u_{y_3} + x^2\,u_{y_4} + xz\,u_{y_5} + z^2 + e^{1\left(\frac{x}{a}\right)}u_{y_6} + e^{\left(1\frac{z}{b}\right)}u_{y_7} + \sin\left(3\frac{\pi x}{a}\right)u_{y_8}\\
u_z &= u_{z_1} + x\,u_{z_2} + z\,u_{z_3} + x^2\,u_{z_4} + xz\,u_{z_5} + z^2 + e^{\left(1\frac{x}{a}\right)}u_{z_6} + e^{\left(1\frac{z}{b}\right)}u_{z_7} + \sin\left(3\frac{\pi x}{a}\right)u_{z_8}
\end{aligned}$$

Further expansions are evaluated in the results section. The use of the 2D polynomials $x^i z^j$ allows one to write the so-called Taylor-like expansions (i and j are positive integers). For example, the second-order displacement field is:

$$\begin{aligned}
u_x &= u_{x_1} + x\,u_{x_2} + z\,u_{x_3} + x^2\,u_{x_4} + xz\,u_{x_5} + z^2\,u_{x_6}\\
u_y &= u_{y_1} + x\,u_{y_2} + z\,u_{y_3} + x^2\,u_{y_4} + xz\,u_{y_5} + z^2\,u_{y_6}\\
u_z &= u_{z_1} + x\,u_{z_2} + z\,u_{z_3} + x^2\,u_{z_4} + xz\,u_{z_5} + z^2\,u_{z_6}
\end{aligned} \tag{2}$$

while the third-order one becomes:

$$\begin{aligned}
u_x &= u_{x_1} + x\,u_{x_2} + z\,u_{x_3} + x^2\,u_{x_4} + xz\,u_{x_5} + z^2\,u_{x_6} + x^3\,u_{x_7} + x^2z\,u_{x_8} + xz^2\,u_{x_9} + z^3\,u_{x_{10}}\\
u_y &= u_{y_1} + x\,u_{y_2} + z\,u_{y_3} + x^2\,u_{y_4} + xz\,u_{y_5} + z^2\,u_{y_6} + x^3\,u_{y_7} + x^2z\,u_{y_8} + xz^2\,u_{y_9} + z^3\,u_{y_{10}}\\
u_z &= u_{z_1} + x\,u_{z_2} + z\,u_{z_3} + x^2\,u_{z_4} + xz\,u_{z_5} + z^2\,u_{z_6} + x^3\,u_{z_7} + x^2z\,u_{z_8} + xz^2\,u_{z_9} + z^3\,u_{z_{10}}
\end{aligned} \tag{3}$$

Eqs. (2) and (3) are indicated as TE2 and TE3, and the numbers are the highest exponents of the expressions. A remarkable feature of these expansions is that classical beam theories are obtainable as particular cases. It should be noted that classical theories require reduced material stiffness coefficients to contrast Poisson's locking and, for this reason, for classical and first-order models Poisson's locking is corrected according to Carrera et al. [21]. In addition, with the purpose of reproducing the zig-zag form for the displacements of laminated FG structures, it is possible to introduce the well-known Murakami's function:

$$\begin{aligned}
u_x &= u_{x_1} + x\,u_{x_2} + z\,u_{x_3} + x^2\,u_{x_4} + xz\,u_{x_5} + z^2\,u_{x_6} + (-1)^k\zeta_k u_{x_{7Z}}\\
u_y &= u_{y_1} + x\,u_{y_2} + z\,u_{y_3} + x^2\,u_{y_4} + xz\,u_{y_5} + z^2\,u_{y_6} + (-1)^k\zeta_k u_{y_{7Z}}\\
u_z &= u_{z_1} + x\,u_{z_2} + z\,u_{z_3} + x^2\,u_{z_4} + xz\,u_{z_5} + z^2\,u_{z_6} + (-1)^k\zeta_k u_{z_{7Z}}
\end{aligned} \tag{4}$$

where $\zeta_k = 2z_k/h_k$ is a non-dimensional layer coordinate and h_k the thickness of the $k-layer$. The exponent k changes the sign of the zig-zag term in each layer. In this case, the acronym becomes TE2^{ZZ}.

3. The FE formulation and preliminaries

Adopting the classical Finite Element technique, it is possible to consider arbitrary shaped cross-sections and boundary conditions. The generalized displacement vector is defined as follow:

$$\mathbf{u}_\tau(y) = N_i(y)\mathbf{q}_{\tau i} \tag{5}$$

where $\mathbf{q}_{\tau i}$ is the nodal displacement vector:

$$\mathbf{q}_{\tau i} = \left\{ q_{u_{x_{\tau i}}} \quad q_{u_{y_{\tau i}}} \quad q_{u_{z_{\tau i}}} \right\}^T \tag{6}$$

The Lagrange shape functions N_i are listed in [21] (§5.2.2), for the beam elements with 2, 3 and 4 nodes. In this paper, the elements with four nodes (B4) are used and, therefore, a cubic approximation

along the y axis is obtained. Both stiffness and mass matrix as well as the external loadings are derived via the Principle of Virtual Displacements:

$$\delta L_{int} = \delta L_{ext} + \delta L_{ine} \tag{7}$$

where L_{int} and L_{ine} are the strain energy and the work of inertial loadings, respectively, whereas L_{ext} is the work of external loadings and δ stands for virtual variation. If the work of external loadings is null, Eq. (7) becomes:

$$\delta L_{ine} - \delta L_{int} = \int_V (\delta \boldsymbol{u}^T \rho \ddot{\boldsymbol{u}}) dV - \int_V (\delta \boldsymbol{\epsilon}_p^T \boldsymbol{\sigma}_p + \delta \boldsymbol{\epsilon}_n^T \boldsymbol{\sigma}_n) dV = 0 \tag{8}$$

in which the vector $\ddot{\boldsymbol{u}}$ is the acceleration vector. In order to separate the components which lay on the cross-sections ("p") from those on the planes orthogonal to them ("n"), both stresses and strains are grouped into the following vectors:

$$\begin{aligned} \boldsymbol{\sigma}_p &= \{\, \sigma_{zz} \quad \sigma_{xx} \quad \sigma_{zx} \,\}^T, \quad \boldsymbol{\epsilon}_p = \{\, \epsilon_{zz} \quad \epsilon_{xx} \quad \epsilon_{zx} \,\}^T \\ \boldsymbol{\sigma}_n &= \{\, \sigma_{zy} \quad \sigma_{xy} \quad \sigma_{yy} \,\}^T, \quad \boldsymbol{\epsilon}_n = \{\, \epsilon_{zy} \quad \epsilon_{xy} \quad \epsilon_{yy} \,\}^T \end{aligned} \tag{9}$$

Under the hypothesis of linear analysis and linear elastic material, the strain–displacement relations and the Hooke's law are, respectively:

$$\begin{aligned} \boldsymbol{\epsilon}_p &= \boldsymbol{D_p} \boldsymbol{u} \\ \boldsymbol{\epsilon}_n &= (\boldsymbol{D_{ny}} + \boldsymbol{D_{n\Omega}}) \boldsymbol{u} \end{aligned} \tag{10}$$

$$\begin{aligned} \boldsymbol{\sigma}_p &= C_{pp} \boldsymbol{\epsilon}_p + C_{pn} \boldsymbol{\epsilon}_n \\ \boldsymbol{\sigma}_n &= C_{np} \boldsymbol{\epsilon}_p + C_{nn} \boldsymbol{\epsilon}_n \end{aligned} \tag{11}$$

The differential operators $\boldsymbol{D_p}, \boldsymbol{D_{ny}}$ and $\boldsymbol{D_{n\Omega}}$ are shown in [21] (§5.2.1). For the isotropic materials, the matrices $C_{pp}, \boldsymbol{C}_{pn}$ ($=\boldsymbol{C}_{np}^T$) and C_{nn} are:

$$\boldsymbol{C}_{pp}^k = \begin{bmatrix} \widetilde{C}_{11}^k & \widetilde{C}_{12}^k & 0 \\ \widetilde{C}_{12}^k & \widetilde{C}_{22}^k & 0 \\ 0 & 0 & \widetilde{C}_{66}^k \end{bmatrix}, \quad \boldsymbol{C}_{pn}^k = \begin{bmatrix} 0 & 0 & \widetilde{C}_{13}^k \\ 0 & 0 & \widetilde{C}_{23}^k \\ 0 & 0 & 0 \end{bmatrix}, \quad \boldsymbol{C}_{nn}^k = \begin{bmatrix} \widetilde{C}_{55}^k & 0 & 0 \\ 0 & \widetilde{C}_{44}^k & 0 \\ 0 & 0 & \widetilde{C}_{33} \end{bmatrix} \tag{12}$$

Considering the FGM, since the Young's modulus (E) and the Poisson's ratio (ν) are functions of the coordinates (x,y,z), the coefficients $\widetilde{C}_{ij}^k(x,y,z)$ vary with the position according to the following formula:

$$\widetilde{C}_{11}^k = \widetilde{C}_{22}^k = \widetilde{C}_{33}^k = \frac{E(1-\nu)}{(1+\nu)(1-2\nu)} \qquad \widetilde{C}_{44}^k = \widetilde{C}_{55}^k = \widetilde{C}_{66}^k = \frac{E}{2(1+\nu)} \tag{13}$$

$$\widetilde{C}_{12}^k = \widetilde{C}_{13}^k = \widetilde{C}_{23}^k = \frac{E\nu}{(1+\nu)(1-2\nu)} \tag{14}$$

The apex "k" refers to the generic piece of the structure, which can be made up of any kind of isotropic material. Clearly, this allows us to investigate composite structure and non-homogeneous sections. The virtual variation of the strain energy is rewritten in a compact format using Eqs. (1), (5), (10) and (11):

$$\delta L_{int} = \delta q_{\tau i}^T \boldsymbol{K}^{ij\tau s} q_{si} \tag{15}$$

The $\boldsymbol{K}^{ij\tau s}$ is the stiffness matrix in the form of the fundamental nucleus which is shown in the following formula:

$$\begin{aligned} \boldsymbol{K}^{ij\tau s} = {} & I_l^{ij} \triangleleft \left(\boldsymbol{D}_{np}^T F_\tau \boldsymbol{I}\right) \left[\widetilde{\boldsymbol{C}}_{np}^k \left(\boldsymbol{D}_p F_s \boldsymbol{I}\right) + \widetilde{\boldsymbol{C}}_{nn}^k \left(\boldsymbol{D}_{np} F_s \boldsymbol{I}\right)\right] \\ & + \left(\boldsymbol{D}_p^T F_\tau \boldsymbol{I}\right) \left[\widetilde{\boldsymbol{C}}_{pp}^k \left(\boldsymbol{D}_p F_s \boldsymbol{I}\right) + \widetilde{\boldsymbol{C}}_{pn}^k \left(\boldsymbol{D}_{np} F_s \boldsymbol{I}\right)\right] \triangleright_\Omega + I_l^{ij,y} \\ & \triangleleft \left[\left(\boldsymbol{D}_{np}^T F_\tau \boldsymbol{I}\right) \widetilde{\boldsymbol{C}}_{nn}^k + \left(\boldsymbol{D}_p^T F_\tau \boldsymbol{I}\right) \widetilde{\boldsymbol{C}}_{pn}^k\right] F_s \triangleright_\Omega \boldsymbol{I}_{\Omega y} + I_l^{i,yj} \boldsymbol{I}_{\Omega y} \\ & \triangleleft F_\tau \left[\widetilde{\boldsymbol{C}}_{np}^k \left(\boldsymbol{D}_p F_s \boldsymbol{I}\right) + \widetilde{\boldsymbol{C}}_{nn}^k \left(\boldsymbol{D}_{np} F_s \boldsymbol{I}\right)\right] \triangleright_\Omega + I_l^{i,yj,y} \boldsymbol{I}_{\Omega y} \\ & \triangleleft F_\tau \widetilde{\boldsymbol{C}}_{nn}^k F_s \triangleright_\Omega \boldsymbol{I}_{\Omega y} \end{aligned} \tag{16}$$

where

$$\boldsymbol{I}_{\Omega y} = \begin{bmatrix} 0 & 0 & 1 \\ 1 & 0 & 0 \\ 0 & 1 & 0 \end{bmatrix} \qquad \triangleleft \ldots \triangleright_\Omega = \int_\Omega \ldots d\Omega \tag{17}$$

$$\left(I_l^{ij}, I_l^{ij,y}, I_l^{i,yj}, I_l^{i,yj,y}\right) = \int_l \left(N_i N_j, N_i N_{j,y}, N_{i,y} N_j, N_{i,y} N_{j,y}\right) dy \tag{18}$$

By using Eqs. (1) and (5), the virtual work of inertial loads in Eq. (8) becomes:

$$\delta L_{ine} = \int_l \delta \boldsymbol{q}_{\tau i}^T \boldsymbol{N}_i \left[\int_\Omega \rho^k (F_\tau \boldsymbol{I})(F_s \boldsymbol{I})\, d\Omega\right] \boldsymbol{N}_j \ddot{\boldsymbol{q}}_{sj}\, dy \tag{19}$$

where $\ddot{\boldsymbol{q}}$ is the nodal acceleration vector and the density ρ^k can change similarly to E and ν. The last equation can be written in the following compact manner:

$$\delta L_{ine} = \int_l \delta \boldsymbol{q}_{\tau i}^T \boldsymbol{M}^{ij\tau s} \ddot{\boldsymbol{q}}_{sj}\, dy \tag{20}$$

where $\boldsymbol{M}^{ij\tau s}$ is the mass matrix in the form of fundamental nucleus. Its components are:

$$\begin{aligned} M_{xx}^{ij\tau s} &= M_{yy}^{ij\tau s} = M_{zz}^{ij\tau s} = I_l^{ij} \triangleleft (F_\tau \rho^k \boldsymbol{I} F_s) \triangleright \\ M_{xy}^{ij\tau s} &= M_{xz}^{ij\tau s} = M_{yx}^{ij\tau s} = M_{yz}^{ij\tau s} = M_{zx}^{ij\tau s} = M_{zy}^{ij\tau s} = 0 \end{aligned} \tag{21}$$

The expressions of the fundamental nuclei do not vary with the changing of the approximation order of the displacement theories indeed, so far, no assumption have been made on the models accuracy. In this way, it is very easy to obtain refined beam models with a completely automatic procedure.

Finally, the undamped dynamic problem is written as it follows:

$$\boldsymbol{M}\ddot{q} + \boldsymbol{K} q = 0 \tag{22}$$

where $\boldsymbol{q}$ is the vector of the nodal unknowns. Introducing harmonic solutions, $\boldsymbol{q} = \boldsymbol{q}_0 e^{i\omega t}$, it is possible to compute the natural frequencies (ω_k) by solving the eigenvalues problem:

$$\left(-\omega_k^2 \boldsymbol{M} + \boldsymbol{K}\right) \boldsymbol{q}_k = 0 \tag{23}$$

where $\boldsymbol{q}_k$ is the kth eigenvector.

4. Numerical results and discussion

4.1. Nomenclature used to denote various expansions

Although only a part of results can be presented in this section, all considered expansions are summarized in Table 1 in which acronyms are introduced. In order to understand their meaning, we may refer to the following short expressions:

- functions with single trigonometric factor:

$$sx = \sin\left(m\frac{\pi x}{a}\right) \quad cx = \cos\left(m\frac{\pi x}{a}\right) \quad sz = \sin\left(n\frac{\pi z}{b}\right) \quad cz = \cos\left(n\frac{\pi z}{b}\right)$$
$$sd = \sin\left(m\frac{\pi xz}{ab}\right) \quad cd = \cos\left(m\frac{\pi xz}{ab}\right)$$

- functions with two trigonometric factors:

$$cc = \cos\left(m\frac{\pi x}{a}\right)\cos\left(n\frac{\pi z}{b}\right) \qquad cs = \cos\left(m\frac{\pi x}{a}\right)\sin\left(n\frac{\pi z}{b}\right)$$
$$sc = \sin\left(m\frac{\pi x}{a}\right)\cos\left(n\frac{\pi z}{b}\right) \qquad ss = \sin\left(m\frac{\pi x}{a}\right)\sin\left(n\frac{\pi z}{b}\right)$$

- hyperbolic functions:

$$chx = \cosh(mx) \qquad shx = \sinh(mx) \qquad chz = \cosh(nz) \qquad shz = \sinh(nz)$$

Table 1
Expansions used in the analyses.

	E1	E2	E3	E4	E5	E6	E7	E8	E9
cost	✓	✓	✓	✓	✓	✓	✓	✓	✓
sx	✓	✓	✓		✓		✓	✓	
cx		✓	✓						
sz	✓	✓	✓		✓		✓	✓	
cz		✓	✓						
sd			✓						
cd			✓						
expx				✓	✓				
expz				✓	✓				
shx						✓	✓		
chx						✓	✓		
shz						✓	✓		
chz						✓	✓		
cc									✓
cs									✓
sc									✓
ss									✓
xz								✓	

- exponential functions:

$$expx = e^{(mx)} \qquad expz = e^{(nz)}$$

- polynomial functions:

$$xz = x^m z^n$$

If Taylor's expansions have been added to displacement fields, their order has been specified by the subscript. For the sake of clarity, in the following is presented the example for the first component of the displacement field $E2_2$:

$$\begin{aligned} u_x = {} & cost\, u_{x_1} + \sin\left(\frac{\pi x}{a}\right) u_{x_2} + \cos\left(\frac{\pi x}{a}\right) u_{x_3} + \sin\left(\frac{\pi z}{b}\right) u_{x_4} \\ & + \cos\left(\frac{\pi z}{b}\right) u_{x_5} + \sin\left(2\frac{\pi x}{a}\right) u_{x_6} + \cos\left(2\frac{\pi x}{a}\right) u_{x_7} + \sin\left(2\frac{\pi z}{b}\right) u_{x_8} \\ & + \cos\left(2\frac{\pi z}{b}\right) u_{x_9} + x\, u_{x_{10}} + z\, u_{x_{11}} + x^2\, u_{x_{12}} + xz\, u_{x_{13}} + z^2\, u_{x_{14}} \end{aligned}$$

Anyway, as said before, the reader can refer to [22,23] for a more detailed description of the displacement fields used.

4.2. The square cross-section FG beam

In order to assess the theory, we consider a square cross-section beam. The structure is made of alumina and steel, whose properties are $E_1 = 390$ GPa, $\nu_1 = 0.25, \rho_1 = 3960$ kg/m^3 and $E_2 = 210$ GPa, $\nu_2 = 0.31, \rho_2 = 7800$ kg/m^3, respectively. With the purpose of enabling a general application of results, they are reported in the following non-dimensional form:

$$\bar{\omega} = 10^2\, \omega\, a \sqrt{\frac{\rho_2}{E_2}}$$

where a is the cross-section dimension and ω is the angular frequency. E, ν and ρ vary according to the power gradation law in Eq. (24) along either z-axis ($\alpha_1 = 0$) or both z and x directions ($\alpha_1 \neq 0$ and $\alpha_2 \neq 0$).

$$f = (f_1 - f_2)\left(\frac{1}{2} - \frac{x}{a}\right)^{\alpha_1}\left(\frac{1}{2} - \frac{z}{a}\right)^{\alpha_2} + f_2 \tag{24}$$

Several length-to-thickness ratios ($L/a = 5, 10, 100$) are considered and the results are compared with those available in [30]. In their analysis, Giunta et al. provided closed form solutions using CUF, and higher-order displacement theories were obtained by adopting Taylor-type expansions: the relative results were assessed with three-dimensional FEM solutions. We discretize each structure by using 10 finite elements with 4 nodes (B4) and both ends are simply supported. As can be seen in Tables 2–6, our results obtained by Taylor-like models strongly agree with the references despite slight differences concerning the axial mode. Furthermore, Tables 5 and 6 show the results related to the E2, E4 and E9 expansions which are explicitly expressed in Eqs. (25)–(27), respectively:

E2-N:

$$\begin{aligned} \mathbf{u}(x,y,z,t) = {} & 1\,\mathbf{u}_1(y,t) + sin\left(m\frac{\pi x}{a}\right)\mathbf{u}_{(4m-2)}(y,t) \\ & + sin\left(m\frac{\pi z}{b}\right)\mathbf{u}_{(4m-1)}(y,t) + cos\left(m\frac{\pi x}{a}\right)\mathbf{u}_{(4m)}(y,t) \\ & + cos\left(m\frac{\pi z}{b}\right)\mathbf{u}_{(4m+1)}(y,t) \end{aligned} \tag{25}$$

E4-N:

$$\mathbf{u}(x,y,z,t) = 1\,\mathbf{u}_1(y,t) + e^{(mx)}\mathbf{u}_{(2m)}(y,t) + e^{(mz)}\mathbf{u}_{(2m+1)}(y,t) \tag{26}$$

Table 2
Dimensionless natural frequencies, $\alpha_1 = 1$ and $\alpha_2 = 0$, $L/a = 100$.

Theory	$\bar{\omega}^a \times 10^2$	$\bar{\omega}^b \times 10^2$	$\bar{\omega}^c \times 10^0$	$\bar{\omega}^d \times 10^0$
EBBT [30]	3.8626	3.9219	–	4.3248
FSDT [30]	3.8622	3.9215	–	4.3239
TE3 [30]	3.8624	3.9214	2.7011	4.3247
TE8 [30]	3.8623	3.9214	2.4861	4.3247
EBBT	3.8626	3.9219	–	4.3250
FSDT	3.8622	3.9215	–	4.3241
TE3	3.8624	3.9214	2.7011	4.3276
TE8	3.8623	3.9214	2.4861	4.3273

EBBT: Euler–Bernoulli Beam Theory. *FSDT*: First-order Shear Deformation Theory.
[a] Bending mode in *yz* plane.
[b] Bending mode in *xy* plane.
[c] Torsional mode.
[d] Axial mode.

Table 3
Dimensionless natural frequencies, $\alpha_1 = 1$ and $\alpha_2 = 0$, $L/a = 10$.

Theory	$\bar{\omega}^a \times 10^1$	$\bar{\omega}^b \times 10^1$	$\bar{\omega}^c \times 10^{-1}$	$\bar{\omega}^d \times 10^{-1}$
EBBT [30]	3.8455	3.9060	–	4.3271
FSDT [30]	3.8076	3.8663	–	4.3203
TE3 [30]	3.8027	3.8574	2.7023	4.3163
TE8 [30]	3.8026	3.8568	2.4874	4.3163
EBBT	3.8455	3.9060	–	4.3251
FSDT	3.8076	3.8663	–	4.3208
TE3	3.8026	3.8574	2.7023	4.3180
TE8	3.8025	3.8568	2.4874	4.3148

EBBT: Euler–Bernoulli Beam Theory. *FSDT*: First-order Shear Deformation Theory.
[a] Bending mode in *yz* plane.
[b] Bending mode in xy plane.
[c] Torsional mode.
[d] Axial mode.

Table 4
Dimensionless natural frequencies, $\alpha_1 = 1$ and $\alpha_2 = 0$, $L/a = 5$.

Theory	$\bar{\omega}^a \times 10^{-1}$	$\bar{\omega}^b \times 10^{-1}$	$\bar{\omega}^c \times 10^{-1}$	$\bar{\omega}^d \times 10^{-1}$
EBBT [30]	1.5179	1.5436	–	8.6680
FSDT [30]	1.4633	1.4861	–	8.6192
TE3 [30]	1.4564	1.4735	5.4117	8.5822
TE8 [30]	1.4562	1.4725	4.9825	8.5819
EBBT	1.5179	1.5436	–	8.6664
FSDT	1.4633	1.4861	–	8.6213
TE3	1.4564	1.4735	5.4117	8.5926
TE8	1.4562	1.4725	4.9824	8.5844

EBBT: Euler–Bernoulli Beam Theory. *FSDT*: First-order Shear Deformation Theory.
[a] Bending mode in *yz* plane.
[b] Bending mode in *xy* plane.
[c] Torsional mode.
[d] Axial mode.

Table 5
Dimensionless natural frequencies, $\alpha_1 = 1$ and $\alpha_2 = 1$, $L/a = 10$.

Theory	$\bar{\omega}^a \times 10^1$	$\bar{\omega}^b \times 10^1$	$\bar{\omega}^c \times 10^{-1}$	$\bar{\omega}^d \times 10^{-1}$	DoF
TE8 [30]	3.2019	3.3597	2.1053	3.6916	
EBBT	3.2386	3.4018	–	3.6973	279
FSDT	3.2072	3.3654	–	3.6949	279
TE3	3.2022	3.3599	2.2880	3.6809	930
TE5	3.2019	3.3597	2.1065	3.6846	1953
TE8	3.2018	3.3597	2.1053	3.6860	4185
E2-6	3.3630	3.4978	2.2910	3.6867	2325
E2-4_2	3.2031	3.3607	2.2910	3.6153	2046
E4-6	3.3632	3.4977	2.2910	3.6930	1209
E9-3	3.2424	3.3982	2.1777	3.6825	4557

EBBT: Euler–Bernoulli Beam Theory. *FSDT*: First-order Shear Deformation Theory.
[a] Bending mode in yz' plane.
[b] Bending mode in xy' plane.
[c] Torsional mode.
[d] Axial mode.

Table 6
Dimensionless natural frequencies, $\alpha_1 = 1$ and $\alpha_2 = 1$, $L/a = 5$.

Theory	$\bar{\omega}^a \times 10^{-1}$	$\bar{\omega}^b \times 10^{-1}$	$\bar{\omega}^c \times 10^{-1}$	$\bar{\omega}^d \times 10^{-1}$	DoF
TE8 [30]	1.2262	1.2838	4.2137	7.3519	
EBBT	1.2791	1.3441	–	7.4023	279
FSDT	1.2338	1.2917	–	7.3796	279
TE3	1.2267	1.2840	4.5790	7.1687	930
TE5	1.2262	1.2838	4.2163	7.3003	1953
TE8	1.2262	1.2838	4.2137	7.4182	4185
E2-6	1.2842	1.3340	4.5850	7.3739	2325
E2-4_2	1.2270	1.2844	4.5848	7.3126	2046
E4-6	1.2842	1.3340	4.5850	7.3610	1209
E9-3	1.2304	1.2878	4.2527	7.2848	4557

EBBT: Euler–Bernoulli Beam Theory. *FSDT*: First-order Shear Deformation Theory.
[a] Bending mode in yz' plane.
[b] Bending mode in xy' plane.
[c] Torsional mode.
[d] Axial mode.

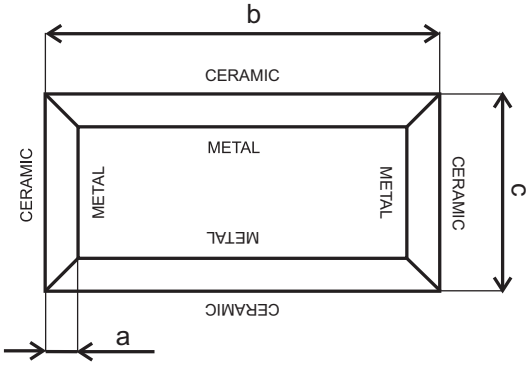

Fig. 1. Sketch of the box beam.

E9-N:

$$\begin{aligned}\mathbf{u}(x,y,z,t) = &\cos\left(m\frac{\pi x}{a}\right)\cos\left(n\frac{\pi z}{b}\right)\mathbf{u}_{m,n}(y,t)\\ &+\cos\left(m\frac{\pi x}{a}\right)\sin\left(n\frac{\pi z}{b}\right)\mathbf{u}_{m,n}(y,t)\\ &+\sin\left(m\frac{\pi x}{a}\right)\cos\left(n\frac{\pi z}{b}\right)\mathbf{u}_{m,n}(y,t)\\ &+\sin\left(m\frac{\pi x}{a}\right)\sin\left(n\frac{\pi z}{b}\right)\mathbf{u}_{m,n}(y,t)\end{aligned} \tag{27}$$

where the indexes m and n indicate summation and go from 1 to N for sinusoidal, cosinusoidal and exponential terms and from 0 to N for trigonometric terms with two factors. The last columns show the number of degrees of freedom[1] (DoF) of the displacement models. It must be underlined that the Taylor-like expansions appear more effective than both trigonometric and exponential series in the computation of the natural frequencies. Indeed, for example, TE5 provides results closer to the reference than to E9 with less than half of DoF.

Table 7
Geometry of box beams.

Parameters	Thin Beam	Thick Beam
L (mm)	762.000	1524.000
a (mm)	0.762	15.240
b (mm)	24.200	106.700
c (mm)	13.600	50.800
Material	CERAMIC	METAL
E (GPa)	380	70
ν	0.3	0.3
rho (kg/m^3)	3800	2707

Table 8
Angular frequencies (rad/s), $\alpha_1 = 1$ and $\alpha_2 = 1$, thin box.

	C–F			C–C		
	ω_z	ω_x	ω_t	ω_z	ω_x	ω_t
FSDT	285.57	446.42	9074.89	1797.73	2791.97	18251.8
[7]	1776.62	2763.49	27234.6	4884.13	7517.71	36523.9
	4917.48	7591.29	45424.3	9399.00	14310.6	54836.7
	9480.03	14487.0	63663.9	15193.3	22851.8	73210.3
3D	283.05	447.19	9030.30	1752.90	2789.90	18057.0
[7]	1758.90	2775.10	27049.0	4764.50	7554.70	36033.0
	4865.90	7654.30	44940.0	9151.60	14467.0	53839.0
	9350.80	14678.0	62610.0	14696.0	23230.0	71381.0
E9-4	292.24	455.76	8863.26	1822.40	2850.26	17019.8[a]
	1797.46	2809.06	24117.6	4942.34	7709.02	29291.3[a]
	4961.42	7738.11	32059.3[a]	9479.46	14756.8	33842.1[a]
	9532.69	14835.1	34592.9[a]	15223.5	23691.6	35966.1[a]
E9-3	381.53	548.93	13902.5	1872.05	2900.01	20034.4[a]
	1918.59	2929.70	26474.6	5020.45	7788.23	31951.5[a]
	5079.11	7854.86	35543.7[a]	9591.93	14861.9	37748.5[a]
	9671.82	14967.1	39196.2[a]	15404.3	23835.9	37979.1[a]
TE6	288.36	451.83	8783.16	1823.41	2849.23	17590.2
	1794.77	2804.89	26286.5	4958.86	7714.73	35054.8
	4972.20	7738.76	43592.4	9556.39	14783.2	52250.7
	9598.18	14855.3	60538.7	15475.0	23781.4	68999.8
TE5	288.37	451.83	8935.69	1823.58	2849.29	17893.7
	1794.87	2804.93	26740.7	4959.85	7715.40	35655.1
	4972.87	7739.34	44337.8	9560.54	14787.2	53134.4
	9601.48	14859.0	61556.9	15488.9	23796.4	70145.1
TE3	288.44	451.86	9761.03	1826.70	2851.27	19553.6
	1796.79	2806.19	29272.4	4976.40	7726.51	39086.9
	4984.36	7747.18	48751.7	9611.63	14821.8	58579.3
	9640.44	14885.6	68177.4	15608.6	23876.9	78010.8
FSDT	287.43	450.31	–	1822.74	2841.45	–
	1796.37	2803.07	–	4999.01	7736.23	–
	5008.10	7765.71	–	9735.23	14923.9	–
	9753.88	14991.7	–	15963.6	23629.3	–

[a] Torsional/shell-like mode.

4.3. The FG box beams

The second assessment regards the dynamic behaviors of thin and thick FGM boxes. Both geometrical and material properties (see Fig. 1 and Table 7) are taken from [7], in which the Dynamic Stiffness Method was used on the basis of first-order shear

[1] $N.DoF = 3 \times N_{nodes} \times T$, in which N_{nodes} is the number of structural nodes and T the number of terms in the expansion.

Table 9
Angular frequencies (rad/s), $\alpha_1 = 0.2$ and $\alpha_2 = 0.2$, thick box.

	C–F			C–C		
	ω_z	ω_x	ω_t	ω_z	ω_x	ω_t
FSDT [7]	242.87	476.97	4821.36	1525.49	2903.00	9765.96
	1507.76	2891.88	14488.2	4130.07	7555.36	19582.1
	4159.85	7716.53	24227.6	7913.11	13861.1	29498.4
	7984.62	14215.5	34087.6	12727.0	21329.7	39564.6
3D [7]	254.13	492.69	4685.00	1584.90	3025.70	9412.00
	1568.10	2998.70	14020.0	4244.50	7932.70	18758.0
	4290.30	8046.00	23250.0	8033.10	14662.0	27973.0
	8145.60	14921.0	32303.0	12749.0	22722.0	36995.0
E9-4	254.57	495.59	4714.85	1572.07	3037.11	9324.41
	1555.58	3007.95	12757.0	4198.87	7951.69	18458.1
	4243.30	8062.62	22800.7	7925.50	14679.1	27371.0
	8036.47	14939.5	31469.0	12545.3	22726.0	35941.4
TE5	252.34	494.21	4676.26	1586.20	3038.66	9414.77
	1562.72	3007.79	14018.3	4275.23	7961.23	18811.8
	4297.73	8068.67	23329.5	8151.97	14706.4	28175.3
	8216.49	14960.5	32590.4	13047.1	22782.3	37492.9
TE3	252.54	494.25	5030.94	1593.72	3039.96	10127.6
	1567.33	3008.56	15092.4	4313.19	7967.56	20256.6
	4324.10	8073.06	25152.8	8263.57	14724.6	30389.3
	8301.92	14974.0	35212.6	13295.3	22822.7	40529.0
TE1	251.33	492.66	6185.38	1586.65	3042.91	12370.7
	1565.10	3014.11	18556.2	4322.87	8047.20	24741.4
	4338.66	8142.64	30926.9	8346.62	15006.2	37112.3
	8382.94	15221.7	43298.0	13544.8	23455.4	49483.8
FSDT	251.33	492.64	–	1586.62	3042.74	–
	1565.08	3014.03	–	4322.80	8046.79	–
	4338.63	8142.43	–	8346.50	15005.5	–
	8382.88	15221.4	–	13544.6	23454.5	–
EBBT	251.53	494.14	–	1599.82	3138.51	–
	1573.61	3075.89	–	4401.62	8582.40	–
	4394.78	8522.01	–	8606.70	16625.8	–
	8582.90	16456.0	–	14186.6	27068.1	–

Table 10
Angular frequencies (rad/s), $\alpha_1 = 10$ and $\alpha_2 = 10$, thick box.

	C–F			C–C		
	ω_z	ω_x	ω_t	ω_z	ω_x	ω_t
FSDT [7]	160.45	300.68	3219.56	1004.50	1826.14	6521.10
	994.04	1820.55	9674.75	2708.56	4741.98	13075.5
	2733.97	4849.14	16178.1	5164.72	8680.42	19696.5
	5225.80	8914.81	22761.7	8262.57	13330.3	26417.2
3D [7]	171.46	322.42	3134.40	1067.40	1974.80	6295.40
	1056.80	1959.10	9377.90	2852.50	5162.40	12543.0
	2886.60	5244.40	15545.0	5385.70	9514.10	18697.0
	5468.70	9700.10	21584.0	8525.60	14705.0	24708.0
E9-4	172.25	324.59	3124.73	1061.08	1983.32	6229.49
	1050.75	1966.23	9237.36	2827.81	5177.21	12329.8
	2861.09	5257.92	15231.1	5324.53	9529.18	18280.9
	5406.69	9723.86	21016.8	8406.56	14712.7	23996.5
TE5	170.65	323.57	3151.68	1071.41	1983.90	6289.06
	1056.03	1965.71	9365.85	2883.36	5181.85	12612.1
	2900.93	5260.44	15582.3	5488.26	9543.00	18810.2
	5537.61	9716.44	21761.1	8766.75	14741.5	25017.2
TE3	170.77	323.60	3368.96	1075.53	1984.99	6779.55
	1058.54	1966.36	10104.9	2903.59	5187.10	13556.9
	2914.94	5264.17	16835.2	5546.79	9557.96	20330.3
	5582.50	9737.94	23556.7	8895.61	14774.2	27099.3
TE1	169.97	322.57	4066.78	1071.89	1988.49	8133.54
	1057.75	1971.07	12200.3	2916.42	5247.09	16267.0
	2929.14	5315.66	20333.8	5621.58	9761.93	24400.6
	5651.32	9916.37	28467.5	9104.84	15223.5	32534.5

deformation theory. The refined beam model takes into account primary and secondary torsional warping and results were compared with three-dimensional finite element solutions, referred here as '3D'. Two boundary conditions are considered: clamped-free (C–F) and clamped–clamped (C–C). Also in this case, the beams are discretized with 10 finite elements B4. The material

Table 11
Properties of the sandwich beams.

Material	Core		Face
	ZIRCONIA	ALUMINUM	STEEL
E (GPa)	151	70	210
v	0.3	0.3	0.3
rho (kg/m^3)	5700	2700	7860

properties change in accordance with the power law (Eq. (24)) considering different values of α_1 and α_2. The angular frequencies (rad/s) related to the flexural modes in z- and x-direction and the torsional modes are indicated as ω_z, ω_x and ω_t, respectively. For the thin box, the results in Table 8 show that the flexural frequencies remain nearly constant and greater than the references, regardless of order and type of expansion. On the contrary, the enrichment of the displacement fields lead the beam elements to detect the torsional frequencies at very different values. Since the structure walls are very thin, the torsional modes can be affected by the shell-like deformations of the cross-section and, for this reason, there can be strong discrepancies in frequency computation (see the theory E9-4). In contrast, for the thick boxes (Tables 9 and 10), the results obtained with the present kinematic models agree with the 3D solutions for all considered conditions. In the case in point, shell deformations are lessened by the considerable thickness of the boxes and, for this reason, even TE5 theory ensures a good accuracy in the computation of the torsional frequencies. Some slight discrepancies between the present results and those proposed in [7] are evident.

4.4. Sandwich beams

In the following case, sandwich beams are considered. These structures consist of two isotropic faces perfectly bonded to a functionally graded core. The mechanical properties of the core vary according to the linear rule of mixture in which the volume fraction of each of the constituent materials is determined by using the power law distribution (Eq. (24)). The core is made up of Zirconia and Aluminum whose properties are shown in Table 11 together with those of the face sheets. The face layer and core thicknesses are 3 and 14 mm, whereas the overall length and width are 200 and 20 mm respectively. The natural frequencies are shown in Table 12 in which those related to the bending modes in z-direction as well as the first axial mode are compared with the solutions found in [11]. Bui et al. developed a meshfree method and validated their results with three-dimensional finite element solutions. The considered boundary condition is clamped-free. The frequencies f computed with the considered expansions agree with the reference solutions in spite of the fact that the theories are extremely different each other. This demonstrates that refining the kinematic theory ensures increasingly better results. Indeed if we look at the torsional frequencies f_t, they appear at lower values when the displacement field is improved. Furthermore, the introduction of the zig-zag term leads to slight improvements in the computation of the bending modes, whereas it is ineffective for the axial and torsional deformations (see the 4th and 5th columns).

4.5. The FG laminated cylinder

In the final example a FGM sandwich cylinder is studied. Referring to Fig. 2, the ratios length-to-mean radius (L/R) and mean radius-to-thickness (R/h) are assumed to be 5 and 10, respectively. The FG core is perfectly bonded to two isotropic faces, whose thicknesses are equal to $h_1 = h_3 = 0.1$ h. The Young's modulus and the mass density of the core vary according to the following formula:

$$f = (f_1 - f_2)\left(\frac{2|\zeta|}{h_2}\right)^{\alpha} + f_2 \tag{28}$$

Table 12
Natural frequencies (Hz), $\alpha_1 = 0$ and $\alpha_2 = 1$, sandwich beam.

	FSDT	TE1^{zz}	TE3	TE3^{zz}	TE5^{zz}	TE8^{zz}	E4-4$_2$	E9-4^{zz}	[11]
f	460.2	459.1	461.9	461.9	461.6	461.6	461.9	462.2	459.4
	2747.9	2710.5	2726.7	2724.7	2720.7	2720.0	2724.3	2720.6	2708.7
	6433.6	6433.6	6455.9	6455.9	6455.1	6455.1	6455.1	6455.1	6440.7
	7197.2	7005.1	7047.9	7037.9	7019.8	7016.7	7035.9	7016.8	6995.8
	13009.7	12484.2	12565.4	12538.7	12490.9	12483.0	12531.7	12482.4	12446.4
	19723.4	18720.6	18853.6	18801.4	18705.8	18690.9	18784.9	18689.4	18659.5
f_t	–	3995.5	3966.8	3966.8	3505.2	3491.3	3973.2	3508.1	–
	–	11986.6	11900.3	11900.3	10517.4	10475.5	11912.9	10477.8	–
	–	19977.6	19834.2	19834.2	17537.9	17464.9	19867.2	17462.4	–

Result not provided by the model.

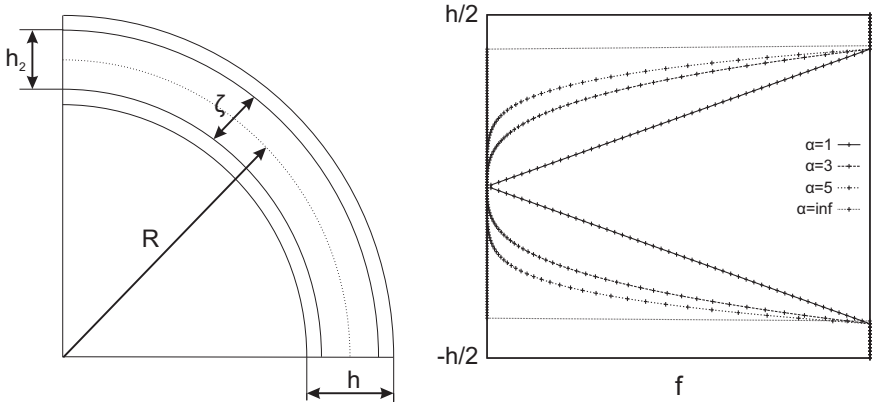

Fig. 2. Cylinder cross-section and variations of the generic property f along the thickness.

Table 13
Non-dimensional frequencies parameter $\bar{\omega}$ for a sandwich FGM cylinder.

α	(m,n)	TE5	TE6	TE8	TE9	TE10	E9-4	LD_{33} [31]
3	(1,1)	0.015361	0.015361	0.015360	0.015360	0.015357	0.015360	0.015396
	(1,2)	0.012379	0.011991	0.010700	0.010572	0.010572	0.010570	0.010603
	(1,3)	0.037004	0.027878	0.023520	0.023487	0.022739	0.023055	0.022764
	(1,4)	0.069182	0.068064	0.050075	0.043592	0.043541	0.043031	0.041413
	(2,1)	0.037971	0.037967	0.037962	0.037962	0.037905	0.037962	0.038044
	(2,2)	0.024680	0.023535	0.022843	0.022764	0.022762	0.022762	0.022814
	(2,3)	0.041048	0.033589	0.028462	0.028326	0.027616	0.027917	0.027637
	(2,4)	0.075675	0.070775	0.053192	0.047022	0.046805	0.046301	0.044643
	(3,1)	0.055409	0.055400	0.055380	0.055379	0.055032	0.055380	0.055498
	(3,2)	0.040272	0.038185	0.037661	0.037585	0.037582	0.037582	0.037661
	(3,3)	0.049534	0.043988	0.037851	0.037544	0.036867	0.037163	0.036897
	(3,4)	0.088012	0.076183	0.059094	0.053461	0.052947	0.052460	0.050754
	(4,1)	0.066753	0.066750	0.066674	0.066672	0.066173	0.066672	0.066811
	(4,2)	0.055221	0.052033	0.051449	0.051352	0.051346	0.051348	0.051442
	(4,3)	0.061498	0.057241	0.049866	0.049301	0.048679	0.048912	0.048636
	(4,4)	0.106066	0.084568	0.067819	0.062819	0.061887	0.061404	0.059622
5	(1,1)	0.014674	0.014673	0.014673	0.014673	0.014672	0.014673	0.014728
	(1,2)	0.012008	0.011629	0.010369	0.010235	0.010236	0.010233	0.010286
	(1,3)	0.036057	0.027151	0.022950	0.022915	0.022153	0.022466	0.022212
	(1,4)	0.067267	0.066243	0.048739	0.042526	0.042470	0.041959	0.040374
	(2,1)	0.036278	0.036273	0.036269	0.036269	0.036271	0.036269	0.036397
	(2,2)	0.023750	0.022622	0.021939	0.021854	0.021853	0.021853	0.021938
	(2,3)	0.039935	0.032645	0.027691	0.027547	0.026820	0.027119	0.026885
	(2,4)	0.073364	0.068858	0.051761	0.045849	0.045614	0.045111	0.043497
	(3,1)	0.052961	0.052952	0.052930	0.052929	0.052798	0.052928	0.053116
	(3,2)	0.038704	0.036648	0.036124	0.036042	0.036013	0.036039	0.036172
	(3,3)	0.048072	0.042645	0.036698	0.036371	0.035691	0.035972	0.035768
	(3,4)	0.084994	0.074066	0.057468	0.052071	0.051528	0.051034	0.049390
	(4,1)	0.063862	0.063859	0.063776	0.063774	0.063708	0.063774	0.063998
	(4,2)	0.053099	0.049964	0.049370	0.049266	0.049261	0.049262	0.049433
	(4,3)	0.059573	0.055414	0.048263	0.047658	0.046905	0.047268	0.047061
	(4,4)	0.102079	0.082142	0.065901	0.061110	0.060092	0.059630	0.057938
∞	(1,1)	0.013160	0.013160	0.013159	0.013159	0.013156	0.013159	0.013170
	(1,2)	0.010916	0.010570	0.009423	0.009302	0.009301	0.009301	0.009304
	(1,3)	0.032905	0.024767	0.020979	0.020948	0.020254	0.020543	0.020239
	(1,4)	0.061290	0.060407	0.044434	0.038878	0.038829	0.038352	0.036854
	(2,1)	0.032540	0.032536	0.032532	0.032532	0.032554	0.032531	0.032555
	(2,2)	0.021441	0.020402	0.019777	0.019701	0.019701	0.019700	0.019710
	(2,3)	0.036398	0.029727	0.025240	0.025120	0.024475	0.024741	0.024440
	(2,4)	0.066673	0.062774	0.047179	0.041896	0.041694	0.041225	0.039696
	(3,1)	0.047522	0.047513	0.047494	0.047494	0.047568	0.047493	0.047526
	(3,2)	0.034903	0.033008	0.032532	0.032459	0.032459	0.032458	0.032473
	(3,3)	0.043723	0.038750	0.033355	0.033070	0.032458	0.032712	0.032423
	(3,4)	0.076978	0.067483	0.052349	0.047532	0.047063	0.046611	0.045042
	(4,1)	0.057351	0.057349	0.057277	0.057277	0.057450	0.057275	0.057310
	(4,2)	0.047908	0.045023	0.044493	0.044403	0.044401	0.044400	0.044410
	(4,3)	0.054100	0.050294	0.043797	0.043275	0.042698	0.042926	0.042609
	(4,4)	0.092171	0.074786	0.059985	0.055719	0.054865	0.054426	0.052797

m: Half-waves in y-direction. n: Half-waves in circumferential direction.

where h_2 is the core thickness, ζ is the generic coordinate ($\frac{-h_2}{2} < \zeta < \frac{h_2}{2}$) and the exponent α assumes the values 3, 5 and ∞. In the case in point, E_1 and E_2 are assumed to be 70 and 380 GPa, whereas the mass densities ρ_1, ρ_2 are 2702 and 3800 kg/m^3, respectively. The Poisson' s ratio ν is constant and equal to 0.3. For sake of clarity, Fig. 2 shows how the properties E and ρ change along the thickness. The results in Table 13 are reported in terms of non-dimensional frequency parameter $\bar{\omega} = \omega h \sqrt{\frac{\rho_2}{E_2}}$ and compared with those presented in [31], in which a semi-analytical solution based on the finite layer method was developed for the simply-supported cylindrical structures. As expected, accuracy improves when the displacement field is enriched. The two graphs of Fig. 3 illustrate how the percentage error ($\frac{(\bar{\omega}-\bar{\omega}_{ref})\times 100}{\bar{\omega}_{ref}}$), relating to the various modal shapes, varies with respect to the number of degrees of freedom (DoF). For both values of the exponent α (3 and ∞), it is possible to note that higher order models are needed to reach acceptable results for all modes of deformation and indeed, by using either the tenth-order Taylor expansion or the E9-4 series, errors remain lower than 5%.

5. Conclusion

In this work, one-dimensional finite elements based on various displacement theories have been employed to perform free vibration analyses of the functionally graded beams. The implementation of the finite elements in accordance with the Carrera Unified Formulation made it possible to consider a great variety of structures and boundary conditions. In the light of the results obtained, the following remarks can be made:

- the invariant properties of CUF make it possible to derive infinite numbers of one dimensional models, without the need for *ad hoc* assumptions;
- when thick sandwich beams as well as thin-walled structures are treated, higher-order theories are mandatory in order to ensure a good accuracy in the computation of the flexural and torsional frequencies;
- the variable kinematic models are able to predict with excellent accuracy the shell-like frequencies for different gradation laws.

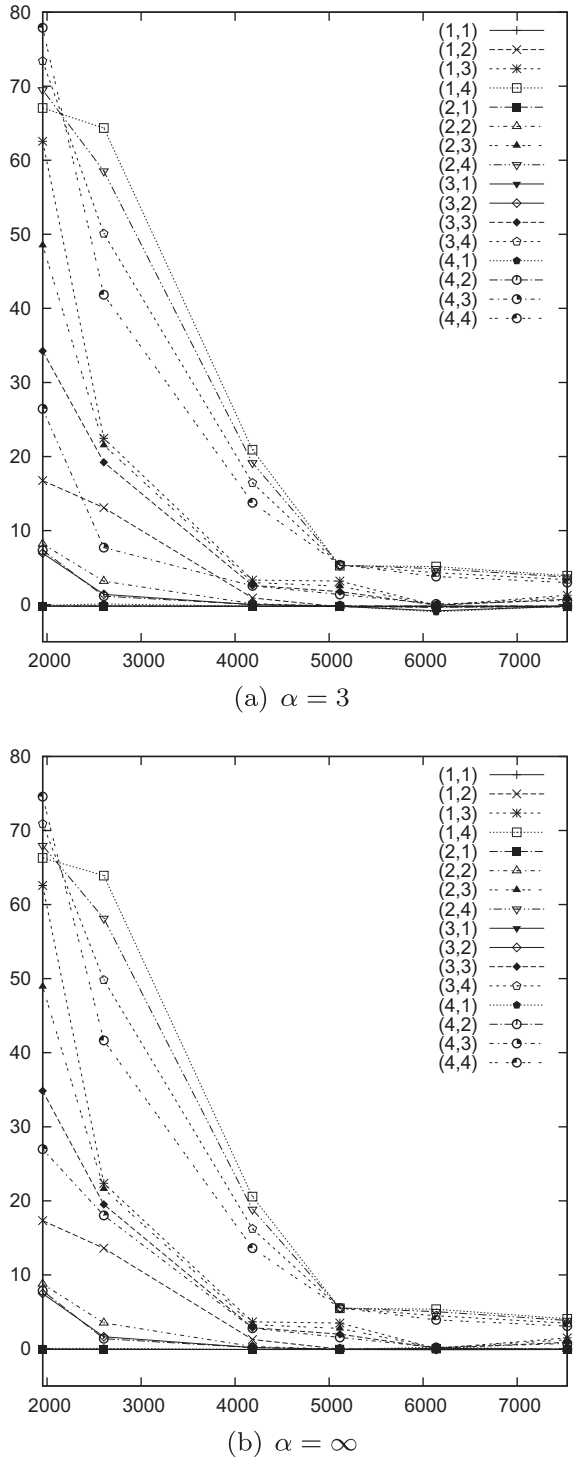

Fig. 3. Percentage error versus the number of degrees of freedom.

In conclusion, the extension of 1D-CUF to the dynamic study of functionally graded structures makes it possible to solve problems which generally require bi- or three-dimensional solutions. Even if the choice of the model is problem-dependent, the possibility to conceive a huge variety of kinematic theories appears to be a remarkable advantage of the proposed formulation. The inclusion of CUF in genetic algorithms could be a suitable approach for comparing several theories for many structural problems. Moreover, future works could investigate the static behaviour of FG structures both in terms of displacements and stress distributions as well as the effect of temperature on fixed and rotating FG beams.

Acknowledgements

This paper was funded by the Deanship of Scientific Research (DSR), King Abdulaziz University, Jeddah, under HiCi 1433130-21 Grant. The authors, therefore, acknowledge with thanks DSR technical and financial support.

References

[1] Aydogdu M, Vedat T. Free vibration analysis of functionally graded beams with simply supported edges. Mater Des 2007;28:1651–6. http://dx.doi.org/10.1016/j.matdes.2006.02.007.
[2] Thai Huu-Tai, Vo Thuc P. Bending and free vibration of functionally graded beams using various higher-order shear deformation beam theories. Int J Mech Sci 2012;62:57–66. http://dx.doi.org/10.1016/j.ijmecsci.2012.05.014.
[3] Simsek M. Fundamental frequency analysis of functionally graded beams by using different higher-order beam theories. Nucl Eng Des 2010;240:697–705. http://dx.doi.org/10.1016/j.nucengdes.2009.12.013.
[4] Li X-F. A unified approach for analyzing static and dynamic behaviors of functionally graded timoshenko and eulerbernoulli beams. J Sound Vib 2008;318:1210–29. http://dx.doi.org/10.1016/j.jsv.2008.04.056.
[5] Sina SA, Navazi HM, Haddadpour H. An analytical method for free vibration analysis of functionally graded beams. Mater Des 2009;30:741–7. http://dx.doi.org/10.1016/j.matdes.2008.05.015.
[6] Pradhan KK, Chakraverty S. Free vibration of euler and timoshenko functionally graded beams by rayleighritz method. Composites: Part B 2013;51:175–84. http://dx.doi.org/10.1016/j.compositesb.2013.02.027.
[7] Ziane N, Meftah SA, Belhadj HA, Tounsi A, Bedia EAA. Free vibration analysis of thin and thick-walled FGM box beams. Int J Mech Sci 2013;66:273–82.
[8] Kapuria S, Bhattacharyya M, Kumar AN. Bending and free vibration response of layered functionally graded beams: a theoretical model and its experimental validation. Compos Struct 2008;82:390–402. http://dx.doi.org/10.1016/j.compstruct.2007.01.019.
[9] Rahmani O, Khalili SMR, Malekzadeh K, Hadavinia H. Free vibration analysis of sandwich structures with a flexible functionally graded syntactic core. Compos Struct 2009;91:229–35. http://dx.doi.org/10.1016/j.compstruct.2009.05.007.
[10] Amirani MC, Khalili SMR, Nemati N. Free vibration analysis of sandwich beam with fg core using the element free galerkin method. Compos Struct 2009;90:373–9. http://dx.doi.org/10.1016/j.compstruct.2009.03.023.
[11] Bui TQ, Khosravifard A, Zhang Ch, Hematiyan MR, Golub MV. Dynamic analysis of sandwich beams with functionally graded core using a truly meshfree radial point interpolation method. Eng Struct 2013;47:90–104. http://dx.doi.org/10.1016/j.engstruct.2012.03.041.
[12] Praveen GN, Reddy JN. Nonlinear transient thermoeastic analysis of functionally graded ceramic-metal plates. Int J Solids Struct 1998;35:4457–76.
[13] Loy CT, Lam KY, Reddy JN. Vibration of functionally graded cylindrical shells. Int J Mech Sci 1999;41:309–24.
[14] Pradham SC, Loy CT, Lam KY, Reddy JN. Vibration characteristics of functionally graded cylindrical shells under various boundary conditions. Appl Acoust 2000;61:111–29.
[15] Qian LF, Batra RC, Chen LM. Static and dynamic deformations of thick functionally graded elastic plates by using higher-order shear and normal deformable plate theory and meshless local petrovgalerkin method. Composites: Part B 2004;35:685–97. http://dx.doi.org/10.1016/j.compositesb.2004.02.004.
[16] Ferreira AJM, Batra RC, Roque CMC, Qian LF, Jorge RMN. Natural frequencies of functionally graded plates by a meshless method. Compos Struct 2006;75:593–600. http://dx.doi.org/10.1016/j.compstruct.2006.04.018.
[17] Matsunaga H. Free vibration and stability of functionally graded plates according to a 2-d higher-order deformation theory. Compos Struct 2008;82:499–512. http://dx.doi.org/10.1016/j.compstruct.2007.01.030.
[18] Tonabene F, Liverani A, Caligiana G. Fgm and laminated doubly curved shells and panels of revolution with a free-form meridian:a 2-d gdq solution for free vibrations. Int J Mech Sci 2011;53:446–70. http://dx.doi.org/10.1016/j.ijmecsci.2011.03.007.
[19] Tonabene F, Ceruti A. Mixed static and dynamic optimization of four-parameter functionally graded completely doubly curved and degenerate shells and panels using GDQ method. Math Problems Eng 2013.
[20] Carrera E. Theories and finite elements for multilayered plates and shells: a unified compact formulation with numerical assessment and benchmarking. Arch Comput Methods Eng 2003;10(3):216–96.
[21] Carrera E, Giunta G, Petrolo M. Beam structures, classical and advanced theories. Wiley; 2011.
[22] Carrera E, Filippi M, Zappino E. Laminated beam analysis by polynomial, trigonometric, exponential and zig-zag theories. Eur J Mech – A/Solids 2013;41:58–69. http://dx.doi.org/10.1016/j.euromechsol.2013.02.006.
[23] Carrera E, Filippi M, Zappino E. Free vibration analysis of laminated beam by polynomial, trigonometric, exponential and zig-zag theories. J Compos Mater 2013.
[24] Carrera E, Filippi M, Zappino E. Free vibration analysis of rotating composite blades via carrera unified formulation. Compos Struct 2013;106:317–25. http://dx.doi.org/10.1016/j.compstruct.2013.05.055.

[25] Carrera E, Zappino E, Filippi M. Free vibration analysis of thin–walled cylinders reinforced with longitudinal and transversal stiffeners. J Vib Acoust 2013;135(1). http://dx.doi.org/10.1115/1.4007559.
[26] Carrera E, Petrolo M, Zappino E. Performance of CUF approach to analyze the structural behavior of slender bodies. J Struct Eng 2012;138:285–98.
[27] Pagani A, Boscolo M, R Banerjee J, Carrera E. Exact dynamic stiffness elements based on one-dimensional higher-order theories for free vibration analysis of solid and thin-walled structures. J Sound Vib 2013;332:6104–27. http://dx.doi.org/10.1016/j.jsv.2013.06.023.
[28] Cinefra M, Soave M. Accurate vibration analysis of multilayered plates made of functionally graded materials. Mech Adv Mater Struct 2011;18:3–13. http://dx.doi.org/10.1080/15376494.2010.519204.
[29] Dozio L. Natural frequencies of sandwich plates with FGM core via variable-kinematics 2-d ritz models. Compos Struct 2013;96:561–8. http://dx.doi.org/10.1016/j.compstruct.2012.08.016.
[30] Giunta G, Crisafulli D, Belouettar S, Carrera E. Hierarchical theories for the free vibration analysis of functionally graded beams. Compos Struct 2011;94:68–74.
[31] Wu CP, Kuo CH. A unified formulation of pvd-based finite cylindrical layer methods for functionally graded material sandwich cylinders. Appl Math Modell 2013;37:916–38. http://dx.doi.org/10.1016/j.apm.2012.03.025.